Nonlinear interactions in an organic polariton condensate

K. S. Daskalakis[1], S. A. Maier[1], R. Murray[1] and S. Kéna-Cohen[1,2†]

[1]Department of Physics

Imperial College London, London, SW7 2AZ

United Kingdom

[2]Department of Engineering Physics

École Polytechnique de Montréal

Montréal, QC, H3C 3A7

Canada

†To whom correspondence should be addressed. E-mail: s.kena-cohen@polymtl.ca

Abstract

Under the right conditions, cavity polaritons form a macroscopic condensate in the ground state. The fascinating nonlinear behaviour of this condensate is largely dictated by the strength of polariton-polariton interactions. In inorganic semiconductors, these result principally from the Coulomb interaction between Wannier-Mott excitons. Such interactions are considerably weaker for the tightly bound Frenkel excitons characteristic of organic semiconductors and were notably absent in the first reported demonstration of organic polariton lasing. In this work, we demonstrate the realization of an organic polariton condensate, at room temperature, in a microcavity containing a thin film of 2,7-bis[9,9-di(4-methylphenyl)-fluoren-2-yl]-9,9-di(4-methylphenyl)fluorene. Upon reaching threshold, we observe the spontaneous formation of a linearly polarized condensate, which exhibits a superlinear power dependence, long-range order and a power dependent blue shift: a clear signature of Frenkel polariton interactions.

The last decade has seen the study of the quantum fluidic behaviour of light flourish.[1] One branch of this field has focused on exploiting the properties of cavity polaritons: hybrid light-matter quasiparticles formed in semiconductor microcavities.[2] The substantial interest in strongly coupled semiconductor microcavities stems principally from the possibility to impart weakly interacting cavity photons with a strongly interacting matter component inherited from the exciton. On one hand, this matter component enhances energetic relaxation towards the polariton ground state by allowing interactions with phonons and other polaritons.[3, 4] On the other hand, the nonlinearity inherited from the exciton gives rise to the hydrodynamic behaviour of polaritons.[5, 6, 7, 8, 9, 10, 11] Polaritons have a finite lifetime, determined principally by their photonic component, beyond which they decay through the cavity mirrors. If relaxation is efficient enough, however, a macroscopic population can be accumulated in a single state—often the ground state—via bosonic final state stimulation.[12, 13, 14] The threshold corresponding to this process, termed polariton lasing, can be significantly below that required for conventional photon lasing. The resulting macroscopically occupied state then behaves as a non-equilibrium Bose-Einstein condensate of polaritons.[15, 16] Although polariton lasing has been mainly observed at low temperature due to the small binding energy typical of Wannier-Mott excitons,[13] recent developments have led to room temperature demonstrations in III-nitrides and ZnO.[17, 18, 19, 20] Frenkel excitons possess binding energies of ~ 1 eV and are thus highly stable at room temperature.[21] Organic polariton lasing was first demonstrated in microcavities containing anthracene single-crystals.[22, 23]

The nonlinear character of polariton condensates leads to a wealth of fascinating phenomena such as superfluidity and the formation of dark solitons and vortices.[7, 8, 9, 10, 11] This nonlinearity, which in a microscopic picture results from polariton-polariton and polariton-exciton interactions,[1, 4, 15, 24] is much weaker for the tightly bound Frenkel excitons characteristic of organic semiconductors and was notably absent in the first reported demonstration of organic polariton lasing.[23] Anthracene does not show the characteristic blue shift that results from strongly interacting polaritons. There, relaxation to the bottom of the lower polariton (LP) branch occurs principally via a resonant process that scatters excitons from the reservoir to a specific energetic point on the LP branch and the observed threshold is determined principally by this single scattering rate.[25] At present, this mechanism is believed to result from the transition dipole moment connecting the vibronic ground state of the first electronically excited state (S_1) to the first vibronic level of the electronic ground state (S_0), the same pathway that leads to stimulated emission in bare anthracene.[26] Thus, the lasing threshold does not differ significantly from that of a conventional laser. This threshold was later shown to decrease by one order of magnitude upon lowering the temperature.[27]

Relaxation via phonon emission and polariton interactions are critical for further reducing the threshold. Polariton-polariton interactions can also dramatically change the spectrum of low energy condensate excitations due to the resulting Bogoliubov dispersion.[28] For Wannier-Mott excitons, exciton-exciton interactions are the result of both the Coulomb interaction between excitons and saturation which arises from the Pauli exclusion principle.[4, 24] For most organic semiconductors, the strength of the Coulomb interaction, which is dominant in the Wannier-Mott case, is weak and depends strongly

on details of the molecular and crystal structure.[29] The saturation term, however, also leads to an effective interaction for Frenkel excitons termed the polariton kinematic interaction. It originates from the fact that two excitons cannot lie on the same lattice site and has been theoretically investigated by several authors.[29, 30, 31] In particular, it has been shown that the paulionic nature of Frenkel excitons leads to an effective *repulsive* interaction.[29, 30]

In the mean field approximation, a generalized Gross-Pitaevskii equation (GPE) can be derived for the condensate wavefunction $\Psi_0(r,t)$:[11, 16]

$$i\hbar\frac{\partial\Psi_0(r,t)}{\partial t}=\left(-\frac{\hbar^2\nabla^2}{2m_{LP}}+\frac{i}{2}\left[W(n_R)-\gamma_{LP}\right]+g\left|\Psi_0(r,t)\right|^2+\tilde{g}n_R\right)\Psi_0(r,t) \qquad (1)$$

where m_{LP} is the LP effective mass, γ_{LP} its decay rate and g is the $k = 0$ value of the effective polariton-polariton interaction potential. Under non-resonant pumping, the condensate interacts with a reservoir of high-energy excitations created by the pump field. In the case of organic microcavities, these resemble bare molecular excitons.[32, 33] They scatter into the condensate with rate $W(n_R)$ and contribute a polariton-exciton interaction constant $\tilde{g}$. A rate equation describes the reservoir occupation, $n_R(t)$:

$$\frac{dn_R(t)}{dt}=P(t)-\frac{n_R(t)}{\tau_R}-k_b{n_R}^2(t)-W(n_R)\left|\Psi_0\right|^2 \qquad (2)$$

where $P(t)$ is the pump rate, τ_R is the reservoir exciton lifetime and k_b is the bimolecular annihilation rate.

In steady-state, the GPE predicts a linear blueshift of the condensate energy $U(n)=gn+\tilde{g}n_R$, where n is the LP density.[1, 15] It is expected that within the pumped region the polariton-exciton interaction principally determines the blue shift.[1, 34] In this

work, we observe the formation of a room temperature organic polariton condensate which, for the first time, exhibits a power-dependent blueshift due to nonlinear interactions between Frenkel excitons. We derive a simple macroscopic model to estimate the polariton-exciton interaction constant.

Linear optical properties

The studied microcavities are shown schematically in Fig. 1a. They are composed of a single film of thermally evaporated 2,7-bis[9,9-di(4-methylphenyl)-fluoren-2-yl]-9,9-di(4-methylphenyl)fluorene (TDAF) sandwiched between two dielectric mirrors. The absorption, photoluminescence and amplified spontaneous emission (ASE) of TDAF are shown in Fig. 1b. The absorption exhibits a strong inhomogeneously broadened excitonic resonance at ~ 3.5 eV. In all-metal microcavities, this material has been used to demonstrate *ultrastrong* coupling with Rabi splittings of $\hbar\Omega \sim 1\,\mathrm{eV}$.[35] It is highly photostable and possesses a quantum efficiency of 0.43. The calculated cavity quality factor for our structure is $Q \sim 300$. From the most negatively detuned photoluminescence linewidth, the measured LP lifetime is estimated to be $\tau_{LP} \sim 55$ fs. This suggests that the kinetics are dominated by single scattering events from the exciton reservoir. For the purpose of this demonstration, the quality factor was deliberately kept low to retain some, albeit weak, visibility for the upper branch in reflectivity due to background absorption on the high energy side of the exciton resonance.

Figure 2 shows a contour map of the transverse electric (TE) and magnetic (TM) angle-resolved reflectivity measured for a 120 nm thick microcavity. The dashed lines trace the fit dispersion of the upper and lower polariton branches, while the circles show

the position of the minima identified on the individual spectra (shown in Supplementary Information). The normal incidence LP energy is obtained from a transmission measurement. The solid black lines show the dispersion of the uncoupled TDAF exciton (E_{ex} = 3.50 eV) and cavity photon obtained from fitting the measured dispersion to a coupled harmonic oscillator model that accounts for the angle-dependence of the DBR penetration depth (see Methods). The resulting fit parameters are shown in the Figure. A giant exciton-photon interaction constant, $V(0)$ = (0.293 ± 0.006) eV, is obtained. It can be related to the Rabi Splitting, Ω, using $\Omega = \sqrt{4V(\theta)^2 - (\gamma_{ex} - \gamma_c)^2}$. Here, $V(\theta)$ is evaluated at the angle, θ, where the exciton and photon are resonant, while γ_{ex} = 240 meV and γ_c = 5 meV are the exciton and photon damping, respectively. Previous studies have shown that the bulky TDAF molecules form disordered films with some slight anisotropy due to a favoured alignment of the molecules with their long axis in-plane.[36] This anisotropy only modifies the TM-polarized photon dispersion for large angles of incidence and was ignored in our modelling.

To obtain the polariton population in the linear regime, we have measured angle-resolved photoluminescence (PL) at low pump fluence. The angle-resolved PL is shown for TM polarization in Fig. 3a and 3b for 120 nm and 140 nm thick microcavities. From the translational invariance of the structure, this emission intensity can be related to the polariton occupation at the corresponding in-plane wavevector k. The detunings, $\Delta = E_{ph}(0) - E_{ex}$, corresponding to the measured sample locations are Δ = - 375 meV and Δ = - 440 meV, respectively and the exciton content, $|X_{LP}|^2$, at the branch minimum is 0.22 and 0.20.

In anthracene microcavities, the emission showed structure mirroring its vibronic progression in PL. In contrast, here, the emission is found to decrease monotonically away from the bottom of the branch, despite the structured nature of the bare TDAF PL. In particular, no peak is observed at ~ 3.05 eV, where the bare PL shows a maximum. For both thicknesses, the resulting dispersion agrees well with that obtained from reflectivity measurements, although small differences occur due to the exact location of the measured spot. The high k region of the branch is thermalized, but this appears to be correlated to the thermalized tail of the bare TDAF PL spectrum. The TE-polarized angle-resolved PL similarly follows the dispersion relation obtained from reflectivity (see Supplementary Information).

Above-threshold behaviour

Upon increasing the pump fluence, a threshold is found which is followed by a superlinear increase in output intensity for TM-polarized emission, regardless of the pump polarization. This increase is accompanied by a blueshift of the emission energy and a collapse, in momentum space, of the emission to the bottom of the LP branch. These two effects are observed in Fig. 3c and 3d, which show the TM-polarized angle-resolved PL measured above threshold for both detunings. We attribute this threshold to the spontaneous formation of a linearly polarized polariton condensate. Note, also, that the emission remains well separated from the bare cavity mode. In real space, a bright spot emerges near the pump centroid with dimensions of approximately one quarter that of the pumped region as shown in Fig. 3e.

The power dependence of the 120 nm-thick microcavity is shown in Fig. 4a. First, we find that at a pump fluence of $P = 4$ μJ/cm^2, the PL transitions from a linear regime, to a sub-linear regime dominated by bimolecular annihilation. Then, at $P_{th} \sim 60$ uJ/cm^2, a superlinear increase in PL intensity is observed, accompanied by a collapse in linewidth, indicative of the increase in temporal coherence. Beyond threshold, we find a *power-dependent blueshift* of the emission energy (shown in the inset), accompanied by significant linewidth broadening. In inorganic microcavities, similar broadening is observed and has been attributed to phase diffusion due to polariton self-interaction within the condensate and to condensation within different localized modes.[37, 38] The individual spectra, measured at normal incidence ($k = 0$), are shown in Fig. 4b. The 140 nm-thick microcavity exhibits a similar power-dependence and blueshift (shown in Supplementary Information). Note that increasing the number of mirror pairs can readily reduce the threshold. Figure 4c shows the power dependence obtained for an identical cavity with 9 mirror pairs ($\tau_{LP} \sim 150$ fs). Here, we find a threshold $P_{th} \sim 30$ uJ/cm^2, concomitant with the longer LP lifetime. For all samples, a blueshift is observed despite the peak in emission and ASE of TDAF lying on red side of the LP ground state. This contrasts with conventional laser frequency pulling where the emission shifts towards the gain maximum. The observed blueshift is a clear signature of polariton-polariton and polariton-exciton interactions. To our knowledge, this is the first time that signatures of such interactions have been observed for tightly bound Frenkel excitons. Note that the large Stokes shift of TDAF inhibits efficient pumping of the LP at energies above that of the vibrationally relaxed electronic excited state. As a result, we only observe lasing for cavities with $\Delta < -320$ meV.

The polarization dependence of the above threshold PL and its color-coded spectral position are shown in Fig. 4d for the 140 nm thick cavity. Below threshold, the emission is completely unpolarized. Above threshold, the emission is almost completely TM-polarized, although weak residual TE emission is present which does not exhibit a blueshift. Because there is no in-plane anisotropy, the spontaneous selection of TM polarization is surprising. For large pump angles, however, the microcavity absorbance is only significant for TM polarization. As a result, the applied electric field on the TDAF molecules is oriented along the TM plane of incidence, *as defined by the pump*, regardless of the net pump polarization. To our knowledge, there have been no studies of the polarization memory of TDAF molecules, but our results suggest that depolarization occurs on a scale longer than the LP lifetime.

To gain insight into the polariton and reservoir dynamics, we have measured time-resolved emission from the LP, shown in Fig. 5. We find that in the linear regime, the LP exhibits biexponential decay with an amplitude-weighted lifetime τ_{exc} = 230 ps. This lifetime is attributed to the exciton reservoir dynamics, which are considerably slower than τ_{LP}. Upon increasing the pump fluence, a fast decay is observed at short times due to bimolecular annihilation, as described by Eq. (2). Above threshold, however, a significant collapse of the emission lifetime results from stimulated scattering to the condensate. Freshly grown TDAF films also exhibit biexponential decay, but with a weighted lifetime τ_{TDAF} = 570 ps. To assess the effect of damage during sputtering of the top mirror, we have measured the lifetime of a control half-cavity (no bottom mirror) to be τ_{HALF} = 330 ps. The reduced lifetime observed for the full cavity, as compared to the control, suggests enhanced scattering of reservoir excitons to the LP. This can occur due

to the emission of optical phonons, on a scale comparable to radiative decay,[39] and via changes in the radiative decay rate due to the modified density of states.[26] Previous reports have observed a weighted lifetime of only 133 ps for bare TDAF films[40]. Here, such short lifetimes have only been observed in the presence of quenching or stimulated emission. Also, the absence of a quadratic power dependence below threshold suggests that pair scattering is not a dominant scattering mechanism in these microcavities.

Long-range spatial coherence

The spontaneous appearance of off-diagonal long-range order is one of the defining features of condensate formation.[37, 41] In the linear regime, polaritons are expected to have a characteristic coherence length on the order of the thermal de Broglie wavelength λ_{dB} = 760 nm. Above threshold, for a homogeneous system, the condensate acquires a constant phase that is spontaneously chosen for each instance of the experiment.[1] The physical manifestation of this long-range order is via the first-order spatial coherence $g^{(1)}(\boldsymbol{r},\boldsymbol{r'})$, which is a measure of the phase coherence between points at $\boldsymbol{r}$ and $\boldsymbol{r'}$. Inhomogeneous pumping causes a spread in momentum space and more complex phase patterns to emerge.[42] To probe the emergence of spatial coherence, we have imaged the condensate in a Michelson interferometer with one of the arms replaced by a retroreflector which inverts the image in a centro-symmetrically.[37] The fringe contrast is thus a measure of the phase coherence between points **r** and **–r**, with respect to the spot centre. Figure 6 shows the images recorded below threshold and for three powers above threshold. Below threshold, only a small autocorrelation fringe can be resolved. At threshold, interference fringes begin to emerge from the centre of the image, due to the

Gaussian pump profile. The emission then corresponds to a central condensed region and sub-threshold PL. As the fluence increases to $P > 1.3P_{th}$ fringes are readily identified over the entire condensate area, a clear manifestation of long-range order. The magnitude of $g^{(1)}(\boldsymbol{r},-\boldsymbol{r})$ can be measured via the fringe visibility as a function of phase delay. The shot-to-shot fluctuations smear out the interference pattern as the phase delay is varied, but we obtain a fringe visibility of ~70% within 3 μm of the centre point.

Blueshift model

To model the blueshift and estimate the polariton interaction coefficients, we use a macroscopic model that includes only the nonlinearity due to exciton saturation.[28] We have measured the polariton occupation at threshold to be $\langle n_{LP} \rangle \sim 7$ per state (see Methods) and the occupation above threshold is simply this number scaled by the observed intensity dependence from Fig. 4. The reservoir surface density in the pumped region, however, is on the order of 10^{14} cm^{-2}. It is thus expected that, similarly to inorganic microcavities, the polariton-exciton interaction is dominant in the pumped region. Ground state saturation leads to a modified exciton-photon interaction constant:

$$V(n_R) = V_0 \sqrt{\frac{(1 - n_R / N_0) d}{(L_{DBR} + d)}} \tag{3}$$

where $N_0 \sim 7 \times 10^{20}$ cm^{-3} is the TDAF molecular density, L_{DBR} is the mirror penetration depth, d is the active layer thickness and V_0 is the exciton-photon interaction strength for $d >> L_{DBR}$. The polariton-exciton interaction constant is then:

$$\tilde{g} = \left. \frac{\partial E_{LP}}{\partial n_R} \right|_{n_0} = \frac{V_0^2}{N_0 \left[E_{UP}(n_0) - E_{LP}(n_0) \right]} \frac{d}{L_{DBR} + d} \tag{4}$$

where $E_{UP}(n_0)$ and $E_{LP}(n_0)$ are the UP and LP energies evaluated at the reservoir density linearization point n_0. Putting in typical numbers for our microcavity gives $\tilde{g} \sim 2 \times 10^{-22}$ eV cm^3 for small n_0 and Hartree-Fock theory predicts $g = \tilde{g}/2d|X_{LP}|^2$.[16] One can show that this value translates to an effective nonlinearity several orders of magnitude lower than that of Wannier-Mott excitons.[43] The inset of Fig. 4a compares a calculation of the time-averaged blueshift anticipated for the 120 nm thick microcavity under pulsed excitation (see Methods for details). There is good qualitative agreement with experiment given the absence of any fit parameters, the simplified description of bimolecular annihilation and the assumption of a spatially uniform pump. The Gaussian pump profile, for example, leads to a factor of ~2 difference between the on and off-axis irradiance. Note also the anticipated saturation due to clamping of the reservoir density above threshold. The absence of a measurable blueshift in anthracene microcavities is most likely due to its high molecular density and efficient bimolecular annihilation, which inhibit the build-up of a significant reservoir exciton population.

The macroscopic picture highlights that strong coupling resonantly enhances the nonlinearity arising from ground state depletion. It also shows that a stronger blueshift is anticipated for cavities operating close to saturation. The 9 pair cavity of Fig. 4c, for example, exhibits a reduced blueshift of ~ 4 meV, in agreement with its lower threshold. This, however, becomes advantageous when compared to the reduced lasing linewidth of only ~ 1 meV. In the inset, the experimental blueshift is compared to the macroscopic model. The observed blueshift also provides a quantitative measure of the ground state depletion. At the highest intensities, sufficient depletion can lead to a dynamic transition to weak coupling. In these structures, however, the coupling strength is so large that a

violation of the strong coupling criterion would require three quarters of the molecules to be excited. The corresponding pump fluence is far beyond the damage threshold of our samples.

In conclusion we have observed the formation of a linearly polarized organic polariton condensate, in ambient conditions, in a simple microcavity consisting of a thin film of thermally evaporated TDAF. The ambipolar electrical characteristics of this organic semiconductor make it an attractive candidate for direct electrical injection.[44] Moreover, the underlying mechanism for lasing is observed to be qualitatively different from that of anthracene polariton lasers. In particular, we observe lasing for two widely different detunings, separated by ~65 meV. The observed *power-dependent* blueshift is a clear signature of polariton interactions and, to our knowledge, the first time that such interactions have been observed for Frenkel excitons. We have provided a simple model to describe the blueshift as resulting from exciton saturation. We anticipate that this study will motivate experimental efforts to directly observe hydrodynamic effects in organic polariton fluids and stimulate theoretical efforts to further understand the detailed mechanism for interaction. The latter is paramount for further reducing the lasing threshold to a value achievable via direct electrical injection.

Supplementary Information is linked to the online version of this paper at www.nature.com/nmat.

ACKNOWLEDGEMENTS

SKC and SM gratefully acknowledge funding from the UK Engineering and Physical Sciences Research Council via the *Active Plasmonics* programme grant (EP/H000917/1). K.D. and R.M acknowledge support from the European ITN project "Icarus" (237900). The authors would like to thank L. Mazza for a critical reading of the manuscript and I. Carusotto for helpful comments regarding Ref. 16. SKC thanks Imperial College London for the award of a Junior Research Fellowship.

AUTHOR CONTRIBUTIONS

K.D. fabricated and characterised the TDAF microcavities. S.K.C. conceived the project, designed the structures and guided the experiments. K.D. and S.K.C. co-wrote the manuscript and S.M. and R.M. contributed to the draft. All authors contributed to analysis of the data.

ADDITIONAL INFORMATION

The authors declare no competing financial interests. Reprints and permission information is available online at http://npg.nature.com/reprintsandpermissions/. Correspondence and requests for materials should be addressed to S.K.C.

METHODS

Experimental structure

Two microcavities were fabricated, consisting of 120 and 140 nm thick TDAF layers encapsulated by identical distributed Bragg reflectors (DBRs). The DBRs consisted of 6 pairs of silicon dioxide (d = 44 nm) and tantalum pentoxide (d = 68 nm). These thicknesses were carefully chosen to keep both polariton branches within the limited DBR stop band, a challenge due to the large Rabi splitting. The bottom DBRs were fabricated by RF magnetron sputtering on pre-cleaned fused silica substrates. The TDAF layer was then thermally evaporated at a rate of 2 Å/s and a base pressure of $\sim 10^{-7}$ mbar. To finish the structure, the top DBR was sputtered on the TDAF layer, without breaking vacuum. The TDAF was used as received, without further purification. Both samples show detuning variations on the order of ~ 50 meV due to intrinsic thickness variations over the 15 x 15 mm sample size.

All of the thicknesses and refractive indices used in this work were obtained using spectroscopic ellipsometery (JA Woollam VASE).

Characterization

Angle-resolved reflectivity was performed using an ellipsometer operating in reflectometry mode and a 2 mm spot size. Angle-resolved photoluminescence from the microcavities was measured using a spectrometer fiber-coupled to a computer-controlled goniometer. The detection half-angle of the collection lens is $\Delta\theta = 3.5°$. The samples were excited non-resonantly at a 50° angle using TM-polarized 250 fs pulses from an optical parametric amplifier pumped by a regenerative Yb:KGW chirped pulse amplifier.

The observed nonlinearities were reproduced for both $\lambda = 355$ nm (absorbance peak) and $\lambda = 385$ nm (absorbance tail) pump wavelengths, but only when using sub-ns pulses. All of the data presented in this work used $\lambda = 385$ nm excitation. We also reproduced the results using two very different spot sizes (see Supplementary Information) and both yielded almost identical thresholds. Most results shown in this work were obtained using a 233 x 323 μm elliptical pump spot as defined by the beam waist. The smaller spot used was 44 x 61 μm. In that case, the threshold corresponded to a remarkably low 880 pJ of absorbed pump energy. Time-resolved measurements were performed using a Hamamatsu Streakscope with a jitter-limited time resolution of ~ 28 ps.

The fabricated microcavities continue to exhibit lasing behavior, with only small changes in threshold, several months after fabrication. Above 100 $\mu J/cm^2$, the microcavities exhibit photodegradation on the scale of minutes and this photodegradation can be accompanied by a slow blueshift of the LP energy. During our measurements, the microcavities were exposed to high energy pulses for less than one second per data point. The absence of significant photodegradation was confirmed by verifying the absence of hysteresis in the LP energy and emission intensity.

Transverse magnetic polarized light at an incidence angle 50° from the normal was used for pumping. This polarization was chosen to increase the pump absorbance resulting from the TM transparency window of the DBRs for large angles of incidence. The observed results, however, were independent of the pump polarization with the exception of the increase in absolute pump fluence required to achieve threshold.

Spatial coherence measurements were made in the Michelson retroreflector configuration. The condensate emission was collected with a NA=0.42 objective

possessing and sent to a mirror attached to a piezoelectric stage and a retroreflector via a non-polarizing beamsplitter. After returning through the beamsplitter, the two nearly collimated beams were focused onto a CCD using a f = 200 mm lens, thus providing a ~47X magnification. A neutral density filter was placed in one arm to equilibrate the intensities and a 400 nm long-pass filter was used to eliminate any residual pump light.

Coupled Harmonic Oscillator Model

The dispersion relations obtained from reflectivity were fit using a coupled harmonic oscillator model. The corresponding Hamiltonian is:

$$\hat{H} = \begin{pmatrix} E_{ph}(\theta) - i\gamma_c & V(\theta) \\ V(\theta) & E_{ex} - i\gamma_{ex} \end{pmatrix}$$

where $V(\theta)$ is the exciton-photon interaction strength, given in eV, γ_{ex} = 240 meV and γ_c = 5 meV are the exciton and photon damping. The exciton-photon interaction strength depends on angle and polarization via the DBR penetration depth. An approximate expression describing this dependence can be obtained from the semiclassical description of strong coupling (see Supplementary Information):[2]

$$V(\theta) = V_0 \sqrt{\frac{d}{d + L_{DBR}(\theta)}} \tag{5}$$

Expressions for $L_{DBR}(\theta)$ are given in Ref. 45. The cavity photon dispersion $E_{ph}(\theta)$ is approximated using a single effective index such that $E_{ph}(\theta) = E_{ph}(0)\left(1 - \frac{\sin^2\theta}{n_{eff}^2}\right)^{-1/2}$ and the uncoupled exciton energy, E_{ex}, was kept fixed at E_{ex} = 3.50 eV. The use of Eq. (5)

allows for a single model to simultaneously fit dispersion measurements for both polarizations. The resulting fit parameters are given below:

Table 1: Harmonic Oscillator Fit Parameters

Thickness	$E_{ph}(0)$ (eV)	n_{eff} (TE)	n_{eff} (TM)	V_0 (meV)
120 nm	3.19 ± 0.02	1.93 ± 0.05	2.01 ± 0.06	520 ± 10
140 nm	3.07 ± 0.02	2.06 ± 0.05	1.88 ± 0.04	450 ± 10

Note the small change in V_0 and n_{eff} for both microcavities. Indeed, the simple coupled oscillator model does not account for the asymmetric lineshape of the exciton absorption, the change in background refractive index over the ~1 eV range swept by both branches or the weak uniaxial anisotropy.

Ground state occupation

To estimate the polariton occupation per state, we have directly measured the ground state occupation of the 120 nm thick cavity near threshold with a high sensitivity Joulemeter. To maximize the emitted power, a slightly larger pump spot of area A = 1.87 x 10^{-3} cm^{-2} was used and the detector half angle was $\Delta\theta = 3.2°$. At $1.47P_{th}$, the emitted energy, for TM polarization, measured from one side of the sample was 0.14 pJ/pulse. From the measured power dependence and with both emission directions included, this corresponds to 0.038 pJ/pulse at P_{th}. The total number of states within the detection cone can be estimated using:

$$M = \frac{A}{4\pi^2}\pi(k_0\Delta\theta)^2 \qquad (6)$$

where $k_0 = 2\pi/\lambda$. This gives $M \sim 10670$ and we find that at threshold the LP occupation is approximately $\langle n \rangle \sim 7$/state. Note that the intensity distribution over the Gaussian pump spot and the choice of beam waist to define the area induces a factor of ~ 2 uncertainty in this estimate. Threshold, as defined by the GPE in Eq. (1), corresponds to the point where $W(n_r) = \gamma_{LP}$.

Modelling of the power dependence and blueshift

To model the blueshift, the bimolecular annihilation rate, k_b, and reservoir to LP scattering rate, W, are first extracted by fitting the measured power dependence to a two-level model, analogous to conventional laser rate equations, for the volume density of reservoir excitons and surface density of polaritons:[25]

$$\frac{dn_R(t)}{dt} = \left(1 - n_R/N_0\right)P(t) - \frac{n_R(t)}{\tau_R} - k_b {n_R}^2(t) - \frac{W}{d} n_R n_{LP} \tag{7}$$

$$\frac{dn_{LP}}{dt} = W n_R n_{LP} + df\frac{n_R}{\tau_R} - \frac{n_{LP}}{\tau_{LP}} \tag{8}$$

Due to their low density, bimolecular quenching of polaritons is ignored and a constant f, analogous to the spontaneous emission factor, is included to represent the fraction of spontaneous scattering from the reservoir to the LP. A Gaussian pump term, P(t), of 250 fs FWHM is used and saturation is included within the two-level approximation. Experimental values $\tau_{LP} = 55$ fs, $\tau_R = 300$ ps, $N_0 = 7 \times 10^{20}$ cm^{-3} are used. From the fit we obtain $W = 2 \times 10^{-7}$ cm^{3}s^{-1}, $k_b = 4 \times 10^{-10}$ cm^{3}s^{-1}. We use $f = 0.2$, but note that high fluence region in the measured power dependence is limited by saturation in contrast to results obtained for the lower threshold microcavities. This value does not affect the modelled blueshift which depends only on the average reservoir population. Parameters

extracted from the τ_{LP} = 150 fs power dependence are W = 1.3 x 10^{-7} cm^3s^{-1} and the more realistic f = 5 x 10^{-3}.

To model the time-averaged blueshift, we calculate the intensity-averaged reservoir population, n_{avg} :

$$n_{avg} = \frac{\int n_R(t) I_{PL}(t)\, dt}{\int I_{PL}(t)\, dt} \tag{9}$$

and then use Eq. (3) to calculate the resulting blueshift.

REFERENCES

1. Carusotto I, Ciuti C. Quantum fluids of light. *Rev Mod Phys* 2013, **85**(1)**:** 299-366.

2. Kavokin A. *Microcavities*. Oxford University Press: Oxford ; New York, 2007.

3. Savona V, Tassone F, Piermarocchi C, Quattropani A, Schwendimann P. Theory of polariton photoluminescence in arbitrary semiconductor microcavity structures. *Phys Rev B* 1996, **53**(19)**:** 13051-13062.

4. Tassone F, Yamamoto Y. Exciton-exciton scattering dynamics in a semiconductor microcavity and stimulated scattering into polaritons. *Phys Rev B* 1999, **59**(16)**:** 10830-10842.

5. Christmann G, Tosi G, Berloff NG, Tsotsis P, Eldridge PS, Hatzopoulos Z*, et al.* Polariton ring condensates and sunflower ripples in an expanding quantum liquid. *Phys Rev B* 2012, **85**(23)**:** 235303.

6. Sanvitto D, Pigeon S, Amo A, Ballarini D, De Giorgi M, Carusotto I*, et al.* All-optical control of the quantum flow of a polariton condensate. *Nat Photon* 2011, **5**(10)**:** 610-614.

7. Roumpos G, Fraser MD, Loffler A, Hofling S, Forchel A, Yamamoto Y. Single vortex-antivortex pair in an exciton-polariton condensate. *Nat Phys* 2011, **7**(2)**:** 129-133.

8. Amo A, Pigeon S, Sanvitto D, Sala VG, Hivet R, Carusotto I*, et al.* Polariton Superfluids Reveal Quantum Hydrodynamic Solitons. *Science* 2011, **332**(6034)**:** 1167-1170.

9. Amo A, Lefrere J, Pigeon S, Adrados C, Ciuti C, Carusotto I*, et al.* Superfluidity of polaritons in semiconductor microcavities. *Nat Phys* 2009, **5**(11)**:** 805-810.

10. Lagoudakis KG, Wouters M, Richard M, Baas A, Carusotto I, Andre R*, et al.* Quantized vortices in an exciton-polariton condensate. *Nat Phys* 2008, **4**(9)**:** 706-710.

11. Carusotto I, Ciuti C. Probing Microcavity Polariton Superfluidity through Resonant Rayleigh Scattering. *Phys Rev Lett* 2004, **93**(16)**:** 166401.

12. Dang LS, Heger D, André R, Bœuf F, Romestain R. Stimulation of Polariton Photoluminescence in Semiconductor Microcavity. *Phys Rev Lett* 1998, **81**(18)**:** 3920-3923.

13. Deng H, Weihs G, Snoke D, Bloch J, Yamamoto Y. Polariton lasing vs. photon lasing in a semiconductor microcavity. *Proceedings of the National Academy of Sciences* 2003, **100**(26)**:** 15318-15323.

14. Imamoglu A, Ram RJ, Pau S, Yamamoto Y. Nonequilibrium condensates and lasers without inversion: Exciton-polariton lasers. *Phys Rev A* 1996, **53**(6)**:** 4250-4253.

15. Deng H, Haug H, Yamamoto Y. Exciton-polariton Bose-Einstein condensation. *Rev Mod Phys* 2010, **82**(2)**:** 1489-1537.

16. Wouters M, Carusotto I. Excitations in a Nonequilibrium Bose-Einstein Condensate of Exciton Polaritons. *Phys Rev Lett* 2007, **99**(14)**:** 140402.

17. Lu T-C, Lai Y-Y, Lan Y-P, Huang S-W, Chen J-R, Wu Y-C*, et al.* Room temperature polariton lasing vs. photon lasing in a ZnO-based hybrid microcavity. *Opt Express* 2012, **20**(5)**:** 5530-5537.

18. Li F, Orosz L, Kamoun O, Bouchoule S, Brimont C, Disseix P*, et al.* From Excitonic to Photonic Polariton Condensate in a ZnO-Based Microcavity. *Phys Rev Lett* 2013, **110**(19)**:** 196406.

19. Daskalakis KS, Eldridge PS, Christmann G, Trichas E, Murray R, Iliopoulos E*, et al.* All-dielectric GaN microcavity: Strong coupling and lasing at room temperature. *Appl Phys Lett* 2013, **102**(10)**:** 101113-101113.

20. Christopoulos S, von Högersthal GBH, Grundy AJD, Lagoudakis PG, Kavokin AV, Baumberg JJ*, et al.* Room-Temperature Polariton Lasing in Semiconductor Microcavities. *Phys Rev Lett* 2007, **98**(12)**:** 126405.

21. Lidzey DG, Bradley DDC, Skolnick MS, Virgili T, Walker S, Whittaker DM. Strong exciton-photon coupling in an organic semiconductor microcavity. *Nature* 1998, **395**(6697)**:** 53-55.

22. Kéna-Cohen S, Davanço M, Forrest SR. Strong Exciton-Photon Coupling in an Organic Single Crystal Microcavity. *Phys Rev Lett* 2008, **101**(11)**:** 116401.

23. Kéna-Cohen S, Forrest SR. Room-temperature polariton lasing in an organic single-crystal microcavity. *Nat Phot* 2010, **4**(6)**:** 371-375.

24. Ciuti C, Savona V, Piermarocchi C, Quattropani A, Schwendimann P. Role of the exchange of carriers in elastic exciton-exciton scattering in quantum wells. *Phys Rev B* 1998, **58**(12)**:** 7926-7933.

25. Mazza L, Kéna-Cohen S, Michetti P, La Rocca GC. Microscopic theory of polariton lasing via vibronically assisted scattering. *Phys Rev B* 2013, **88**(7)**:** 075321.

26. Mazza L, Fontanesi L, La Rocca GC. Organic-based microcavities with vibronic progressions: Photoluminescence. *Phys Rev B* 2009, **80**(23)**:** 235314.

27. Slootsky M, Zhang Y, Forrest SR. Temperature dependence of polariton lasing in a crystalline anthracene microcavity. *Phys Rev B* 2012, **86**(4)**:** 045312.

28. Utsunomiya S, Tian L, Roumpos G, Lai CW, Kumada N, Fujisawa T*, et al.* Observation of Bogoliubov excitations in exciton-polariton condensates. *Nat Phys* 2008, **4**(9)**:** 700-705.

29. Litinskaya M. Exciton polariton kinematic interaction in crystalline organic microcavities. *Phys Rev B* 2008, **77**(15)**:** 155325.

30. Bittner ER, Silva C. Estimating the conditions for polariton condensation in organic thin-film microcavities. *J Chem Phys* 2012, **136**(3)**:** 034510-034515.

31. Zoubi H, La Rocca GC. Exciton-polariton kinematic interactions in organic microcavities. *Phys Rev B* 2005, **72**(12)**:** 125306.

32. Agranovich VM, Litinskaia M, Lidzey DG. Cavity polaritons in microcavities containing disordered organic semiconductors. *Phys Rev B* 2003, **67**(8)**:** 085311.

33. Michetti P, La Rocca GC. Polariton states in disordered organic microcavities. *Phys Rev B* 2005, **71**(11)**:** 115320.

34. Wouters M, Liew TCH, Savona V. Energy relaxation in one-dimensional polariton condensates. *Phys Rev B* 2010, **82**(24)**:** 245315.

35. Kéna-Cohen S, Maier SA, Bradley DDC. Ultrastrongly Coupled Exciton–Polaritons in Metal-Clad Organic Semiconductor Microcavities. *Advanced Optical Materials* 2013, **1**(11)**:** 827-833.

36. Lin H-W, Lin C-L, Chang H-H, Lin Y-T, Wu C-C, Chen Y-M*, et al.* Anisotropic optical properties and molecular orientation in vacuum-deposited ter(9,9-diarylfluorene)s thin films using spectroscopic ellipsometry. *J Appl Phys* 2004, **95**(3)**:** 881-886.

37. Kasprzak J, Richard M, Kundermann S, Baas A, Jeambrun P, Keeling JMJ*, et al.* Bose-Einstein condensation of exciton polaritons. *Nature* 2006, **443**(7110)**:** 409-414.

38. Porras D, Tejedor C. Linewidth of a polariton laser: Theoretical analysis of self-interaction effects. *Phys Rev B* 2003, **67**(16)**:** 161310.

39. Litinskaya M, Reineker P, Agranovich VM. Fast polariton relaxation in strongly coupled organic microcavities. *J Lumin* 2004, **110**(4)**:** 364-372.

40. Toffanin S, Capelli R, Hwu T-Y, Wong K-T, Plötzing T, Först M*, et al.* Molecular Host−Guest Energy-Transfer System with an Ultralow Amplified Spontaneous Emission Threshold Employing an Ambipolar Semiconducting Host Matrix. *J Phys Chem B* 2009, **114**(1)**:** 120-127.

41. Deng H, Solomon GS, Hey R, Ploog KH, Yamamoto Y. Spatial Coherence of a Polariton Condensate. *Phys Rev Lett* 2007, **99**(12)**:** 126403.

42. Wouters M, Carusotto I, Ciuti C. Spatial and spectral shape of inhomogeneous nonequilibrium exciton-polariton condensates. *Phys Rev B* 2008, **77**(11)**:** 115340.

43. Snoke D. Polariton Condensation and Lasing. *Exciton Polaritons in Microcavities*. Springer, 2012, pp 307-327.

44. Wu CC, Lin YT, Wong KT, Chen RT, Chien YY. Efficient Organic Blue-Light-Emitting Devices with Double Confinement on Terfluorenes with Ambipolar Carrier Transport Properties. *Adv Mater* 2004, **16**(1)**:** 61-65.

45. Panzarini G, Andreani LC, Armitage A, Baxter D, Skolnick MS, Astratov VN*, et al.* Cavity-polariton dispersion and polarization splitting in single and coupled semiconductor microcavities. *Phys Solid State* 1999, **41**(8)**:** 1223-1238.

FIGURE CAPTIONS

Figure 1. Materials and experimental structure. a) Schematic showing the fabricated structure which consists of two dielectric mirrors of alternating tantalum pentoxide (Ta_2O_5) and silicon dioxide (SiO_2) pairs enclosing a single layer of TDAF. The molecular structure of TDAF is shown between the mirrors. b) The photoluminescence (blue) of bare TDAF and its amplified spontaneous emission spectrum (ASE) (red) are shown on the left. Note the presence of vibronic replicas in the emission spectrum and that the ASE peak coincides with the emission maximum. The ASE spectrum was obtained by pumping a neat 120 nm thick TDAF film with an elliptical spot long enough to achieve significant single-pass gain for the waveguided photons. The absorbance of a 60 nm TDAF film is shown on the right (orange). It shows a strong inhomogenously broadened exciton absorbtion band at ~ 3.5 eV.

Figure 2. Angle-resolved reflectivity. Contour maps of the angle-resolved reflectivity are shown for a) TE and b) TM polarization for the 120 nm thick microcavity. The position of individual minima identified on the spectra are shown as yellow dots (see Supplementary Information for individual spectra). The normal incidence LP energy was obtained from a transmission measurement. The points are readily identified for TM polarization, but the upper branch shows very weak contrast for TE polarization. An identical cavity with only 4 top mirror pairs was fabricated to better identify their positions. The dashed lines are a fit of the lower polariton (LP) and upper polariton (UP)

minima to a coupled harmonic oscillator model, while the solid lines show the uncoupled cavity photon (C) and exciton (X) dispersion relations. The fit parameters are given in the inset.

Figure 3. Angle-resolved photoluminescence. Transverse magnetic polarized PL, taken at low pump fluence, is shown for the a) 120 nm thick and b) 140 nm thick microcavities. The detunings, Δ, obtained from a coupled harmonic oscillator fit to the measured dispersion (dashed line) are indicated on the figure. Note the slightly different detuning as compared to reflectivity due to the different spot location. The uncoupled cavity photon dispersion (C) is shown as a solid black line. Note that both exhibit a monotonic decrease in intensity away from the LP minimum. The above threshold PL, for the same spots, is shown in c) and d). The pump fluence for these two measurements was for $P = 1.2P_{th}$ and $P = 1.8P_{th}$, respectively. Note the collapse of the emission to the LP ground state and the blueshift of the emission peak due to polariton interactions. Real space images of the emission shown in e) highlight the collapse of the emission to a central spot near the pump centroid.

Figure 4. Pump fluence and polarization dependence. a) The dependence of the peak PL intensity and linewidth on the absorbed pump fluence is shown for the 120 nm thick microcavity. Note the transition to a sublinear regime at $P = 4$ μJ/cm^2, followed by the threshold at $P = 60$ μJ/cm^2. The corresponding emission spectra are shown in b). Note the blue shift and superlinear increase beyond $P_{th.}$ c) The pump fluence dependence of an identical cavity composed of 9 mirror pairs is shown. Note the reduced lasing threshold

and larger superlinear increase. The insets of a) and c) shown the experimentally observed blueshifts for the corresponding low Q and high Q microcavities, with the LP lifetimes indicated in the figure. The calculated time-averaged blueshift resulting from the use of pulsed excitation is shown using a solid blue line (see Methods for details of the calculation). In the pumped region, the blueshift is attributed principally to polariton-exciton scattering and as a result, a smaller blueshift is anticipated for the high Q cavity. This is indeed observed in both the measurement and calculation. The clamping of the average reservoir exciton density can also be identified in the model. d) The polarization dependence of the emission peak, for $P = 1.6P_{th}$, of the 140 nm thick microcavity. The emission is TM polarized, regardless of the pump polarization. This agrees with the predominantly TM absorption of the structure at 50°. The plot is colour coded and shows the blueshift in emission energy when going from TE to TM polarization with respect to the plane of incidence defined by the TM pump.

Figure 5. Temporally resolved polariton emission. The time-resolved LP emission is shown as a function of increasing pump fluence. In the linear regime, the emission exhibits a biexponential decay with a weighted lifetime τ = 230 ps. The long lifetime is due to the slow decay of the reservoir population. Upon increasing the pump fluence, a fast decay is observed at short times resulting from bimolecular annihilation within the reservoir. Above threshold, however, a much sharper collapse of the emission lifetime ($\tau < 30$ ps) occurs which is attributed to the onset of stimulated scattering to the condensate.

Figure 6. Spatial coherence. These images show the interference pattern recorded in a Michelson retroreflector configuration for various pump fluences. The fringes observed at each point **r** are indicative of the spatial coherence between it and its centro-symmetric counterpart **-r**. A small autocorrelation fringe can be resolved below threshold. As threshold is reached, the emission spot collapses and fringes emerge from the pump centre. Beyond approximately $1.3P_{th}$, fringes are observed over the entire condensate area indicative of macroscopic phase coherence throughout the condensate.

FIGURES

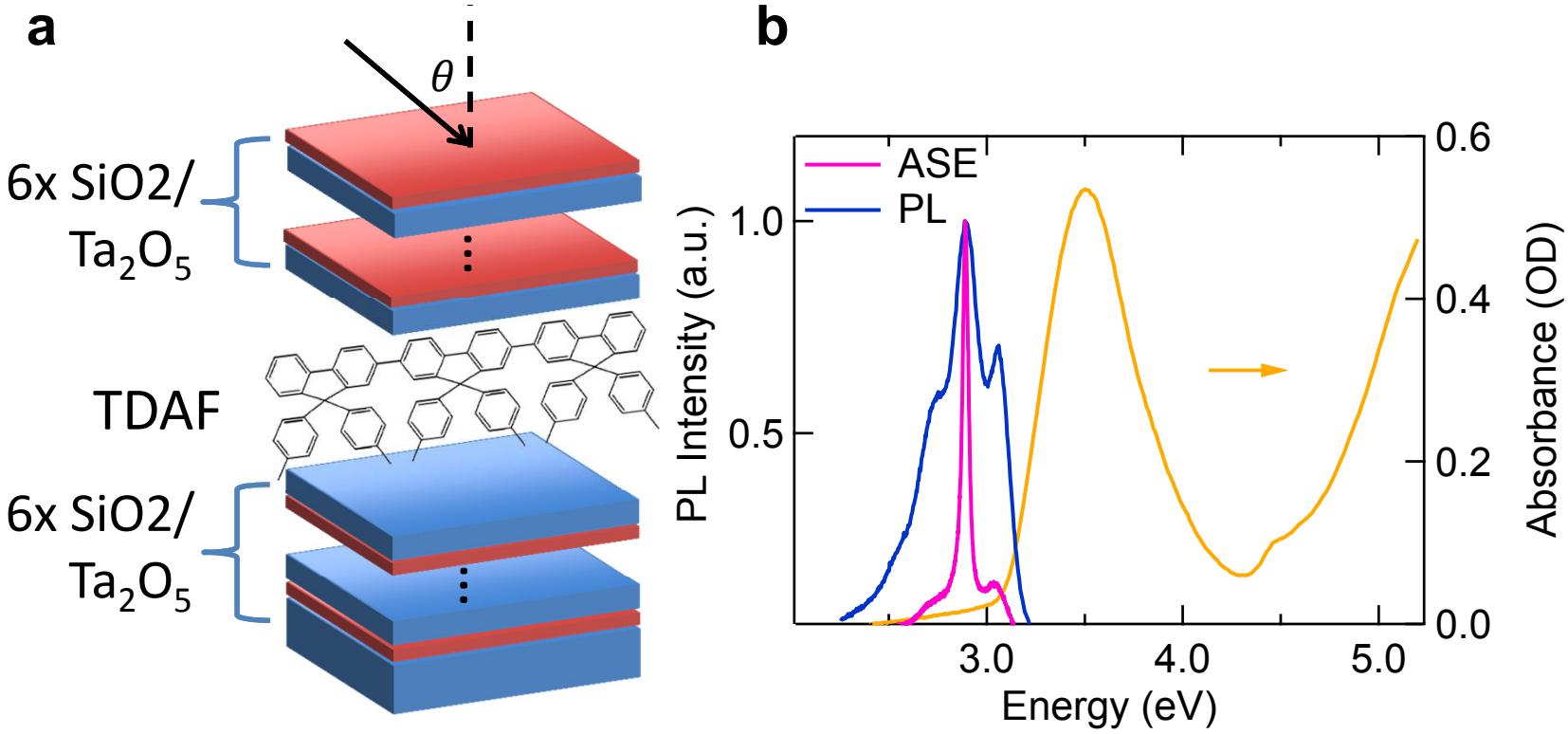

Figure 1 – Daskalakis *et al.*

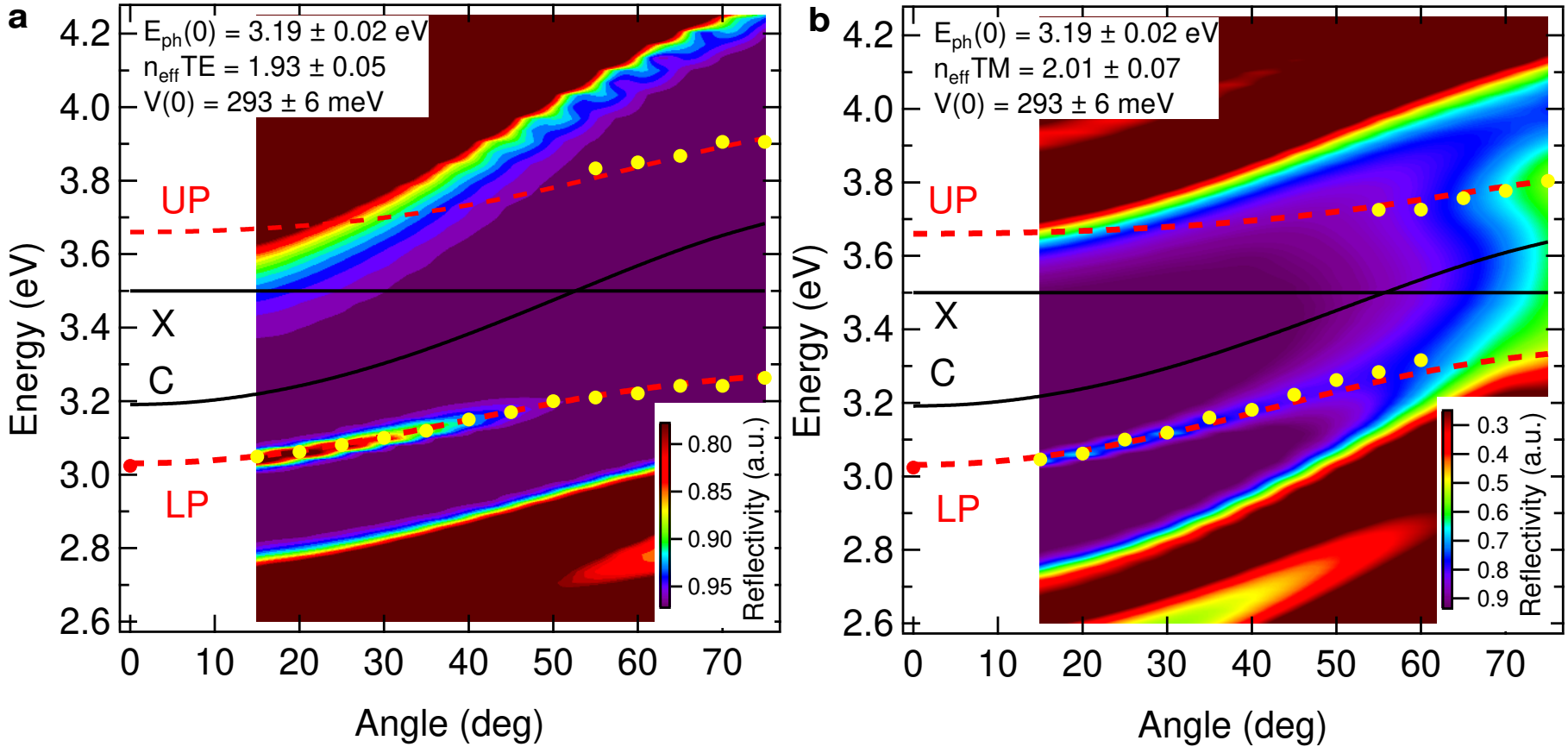
a
$E_{ph}(0)$ = 3.19 ± 0.02 eV
n_{eff}TE = 1.93 ± 0.05
V(0) = 293 ± 6 meV
UP
X
C
LP
Energy (eV)
Angle (deg)
Reflectivity (a.u.)
b
$E_{ph}(0)$ = 3.19 ± 0.02 eV
n_{eff}TM = 2.01 ± 0.07
V(0) = 293 ± 6 meV
UP
X
C
LP
Energy (eV)
Angle (deg)
Reflectivity (a.u.)

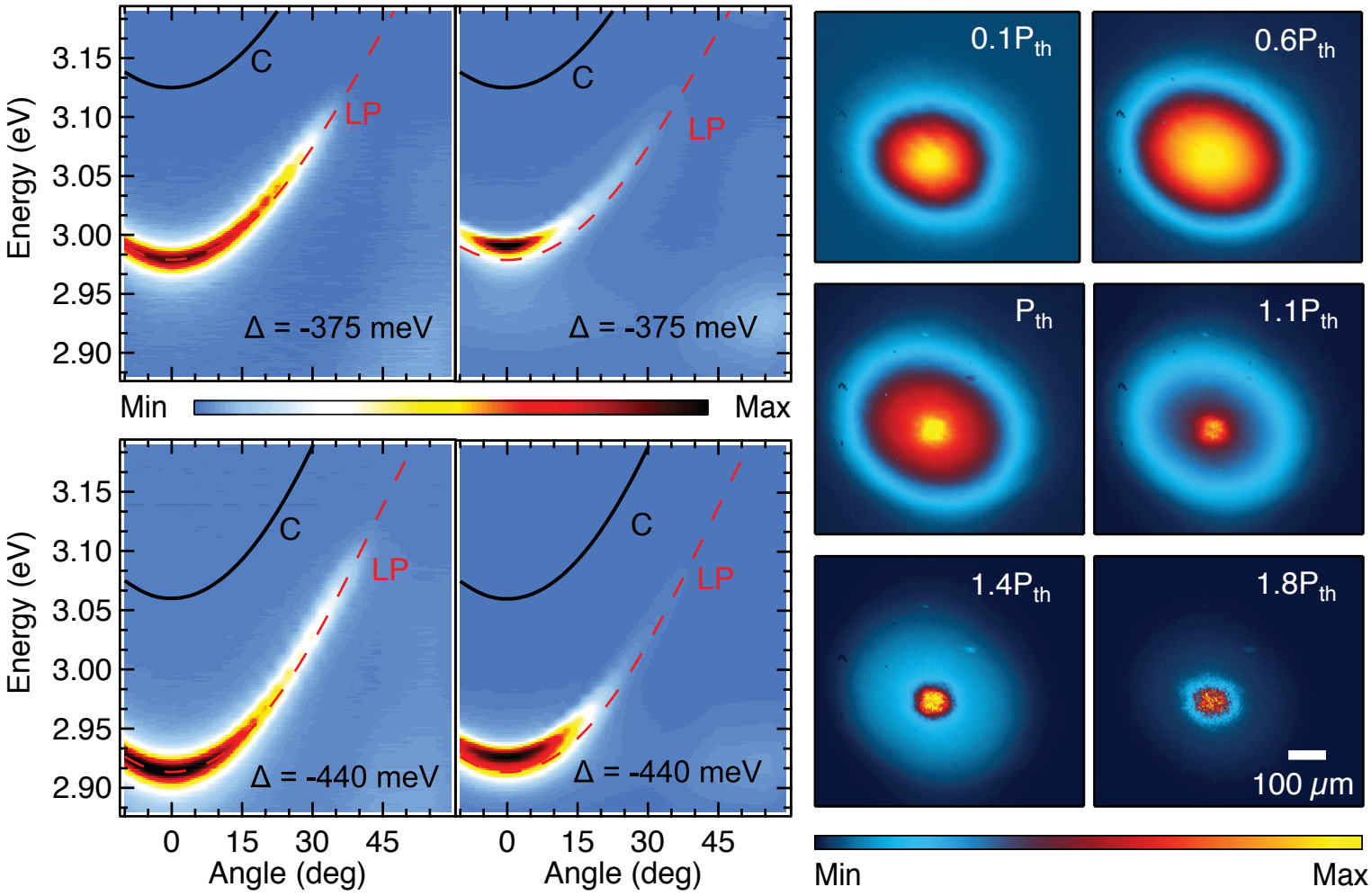

Figure 3 - Daskalakis *et al.*

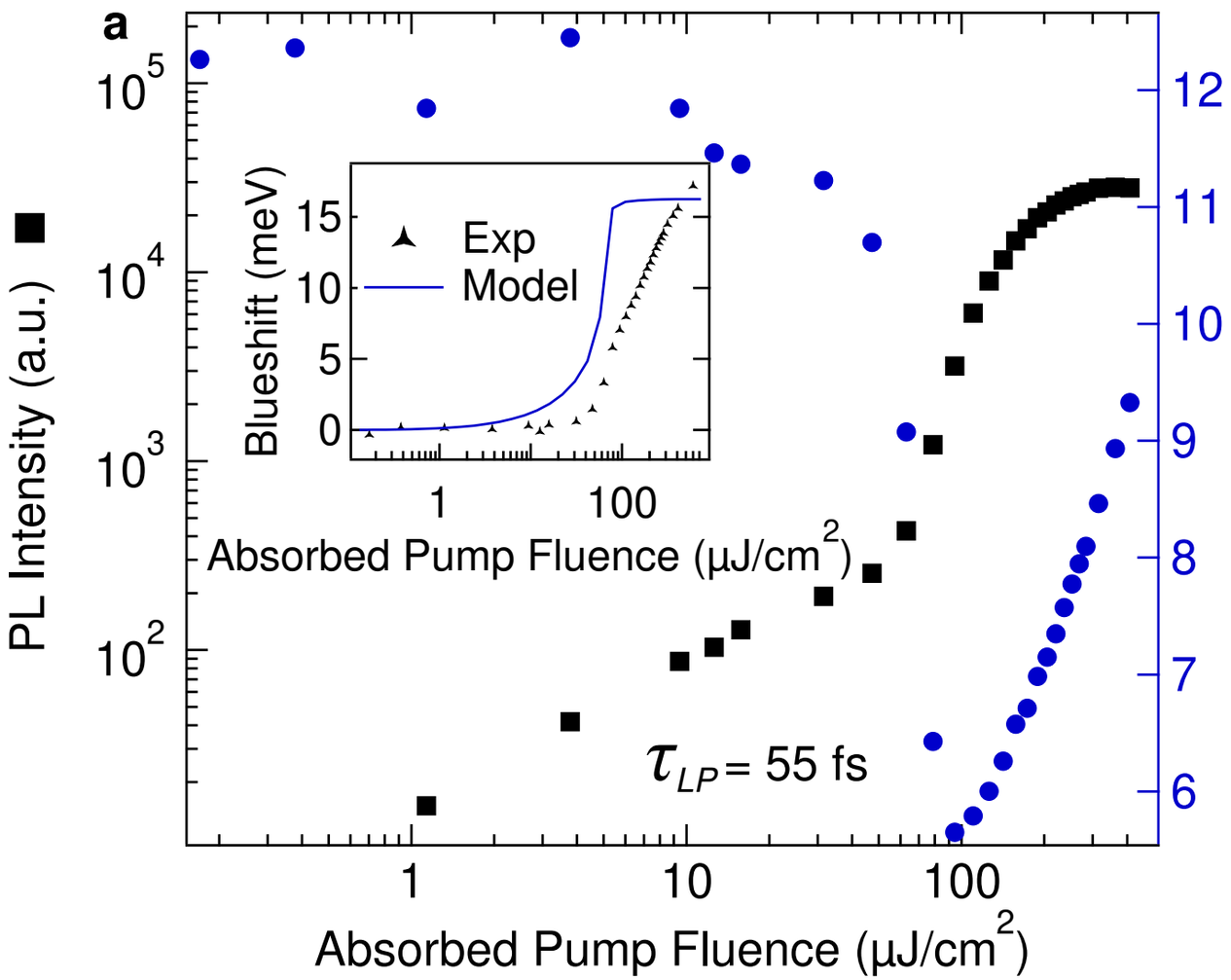
a
PL Intensity (a.u.)
Linewidth (meV)
Blueshift (meV)
Exp
Model
Absorbed Pump Fluence (μJ/cm²)
τ_LP = 55 fs

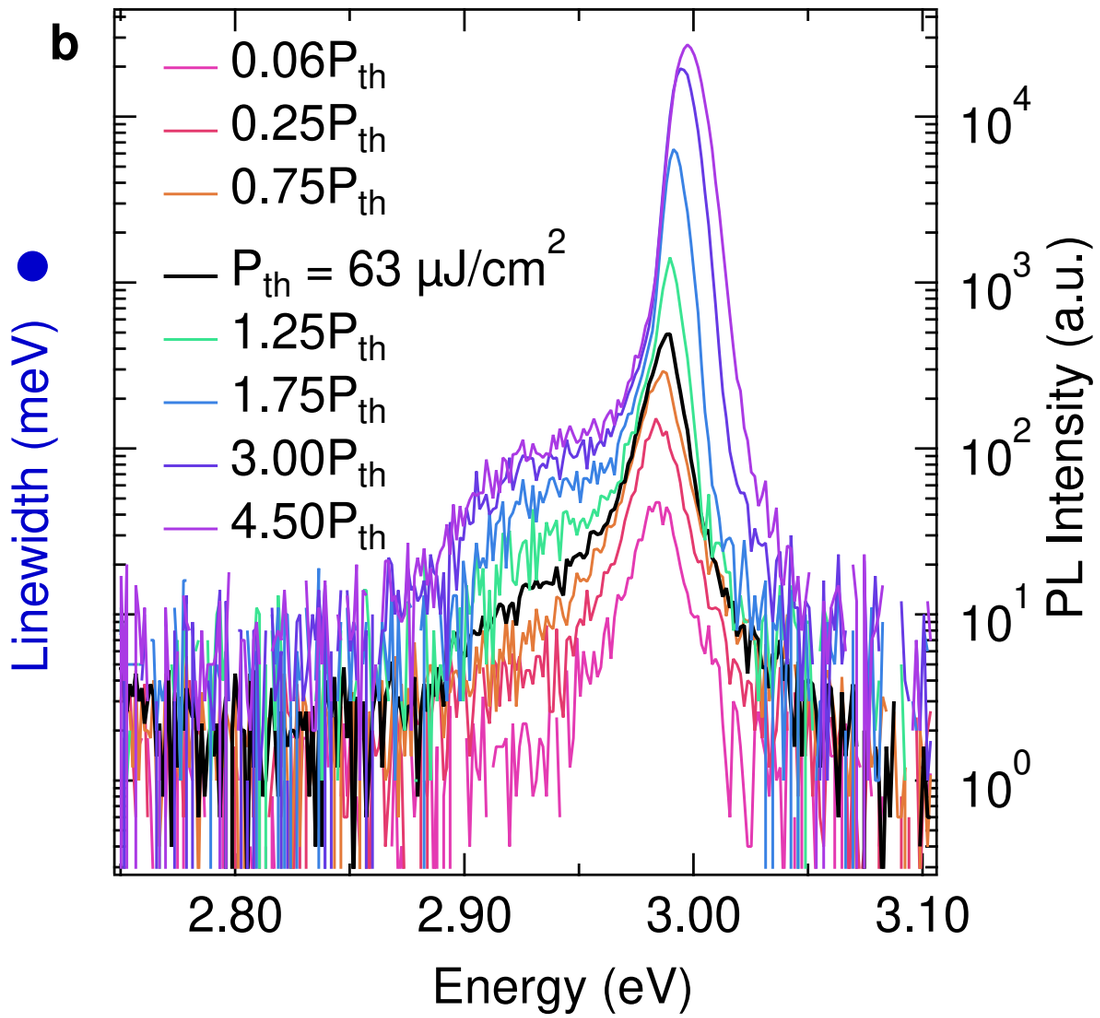
b
0.06P_th
0.25P_th
0.75P_th
P_th = 63 μJ/cm²
1.25P_th
1.75P_th
3.00P_th
4.50P_th
PL Intensity (a.u.)
Energy (eV)

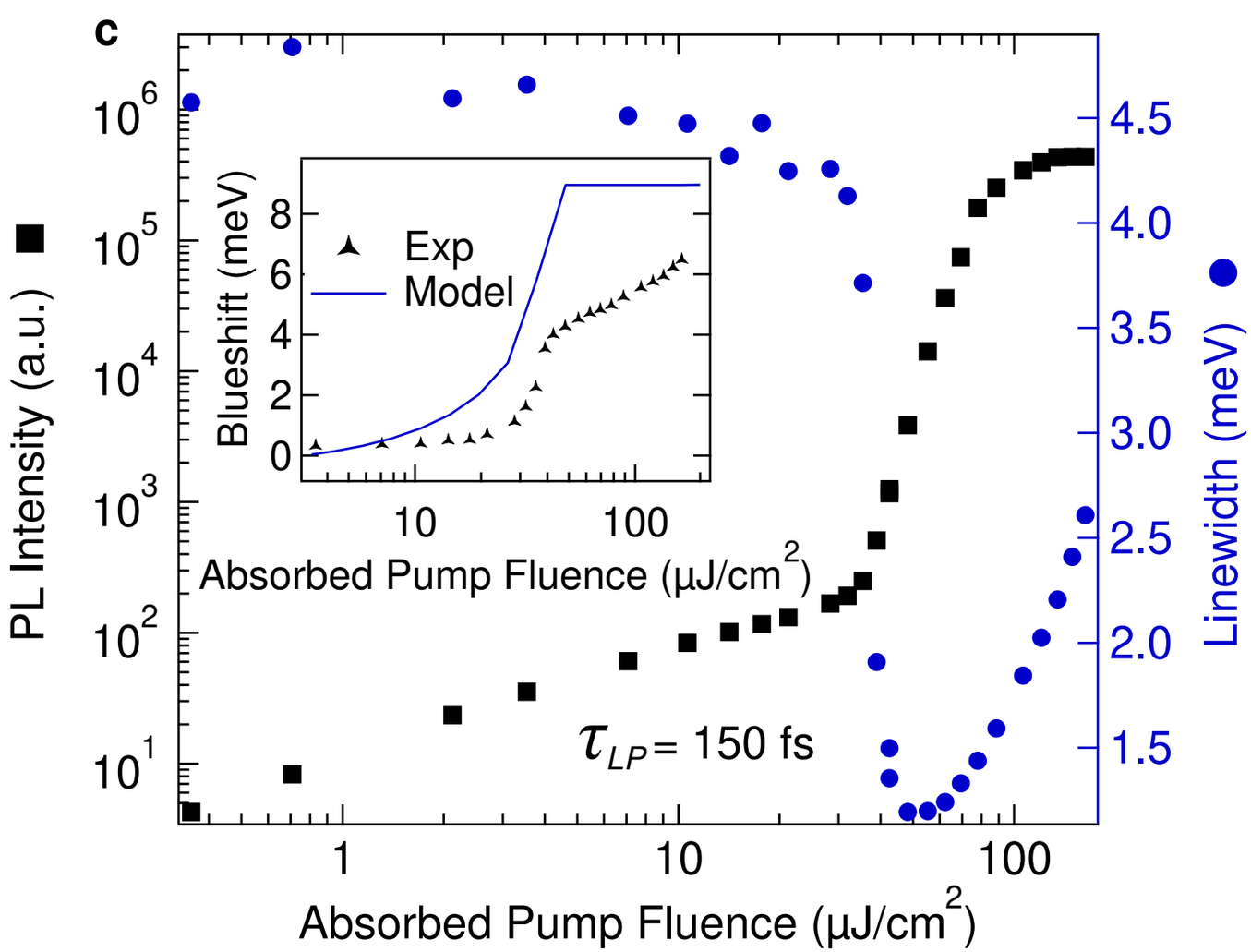
c
PL Intensity (a.u.)
Linewidth (meV)
Blueshift (meV)
Exp
Model
Absorbed Pump Fluence (μJ/cm²)
τ_LP = 150 fs

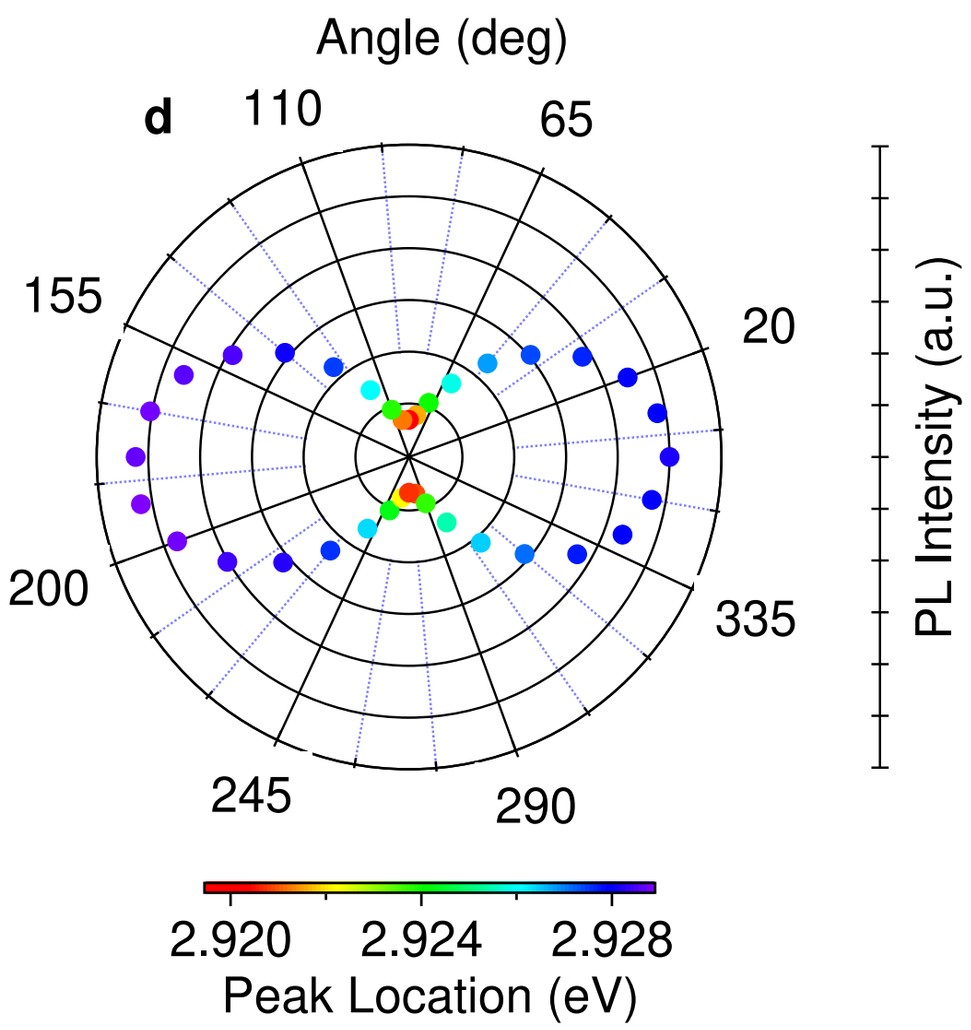
Angle (deg)
d
PL Intensity (a.u.)
Peak Location (eV)

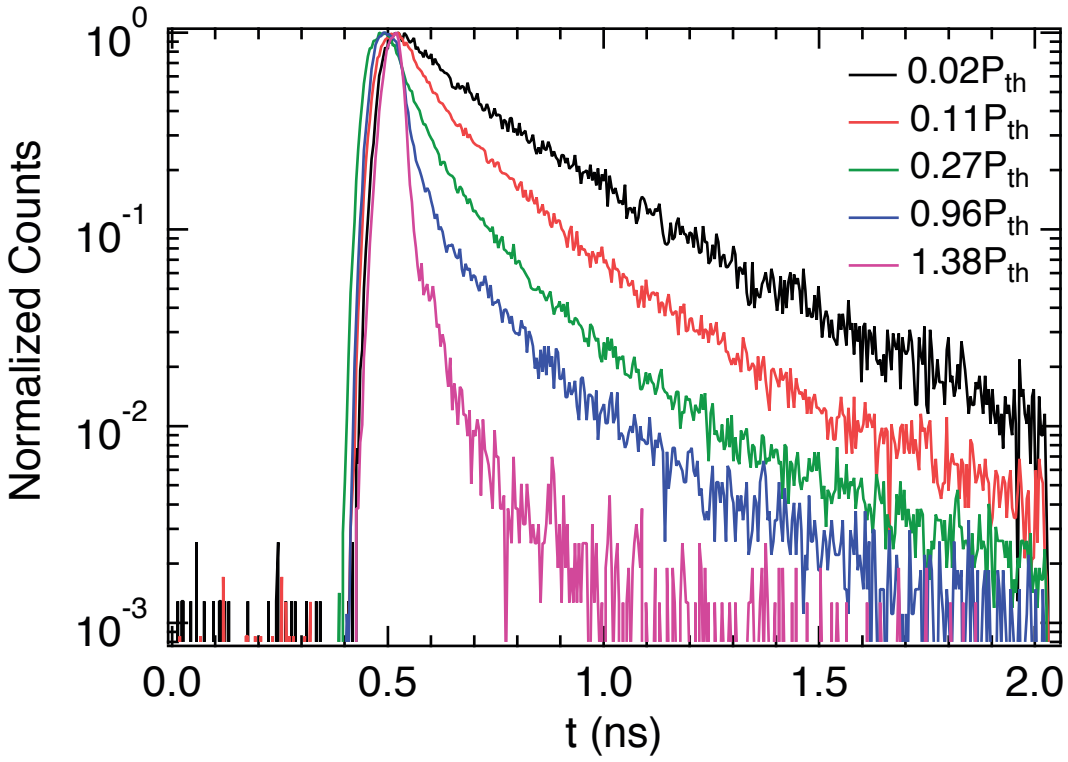

Figure 5 - Daskalakis *et al.*

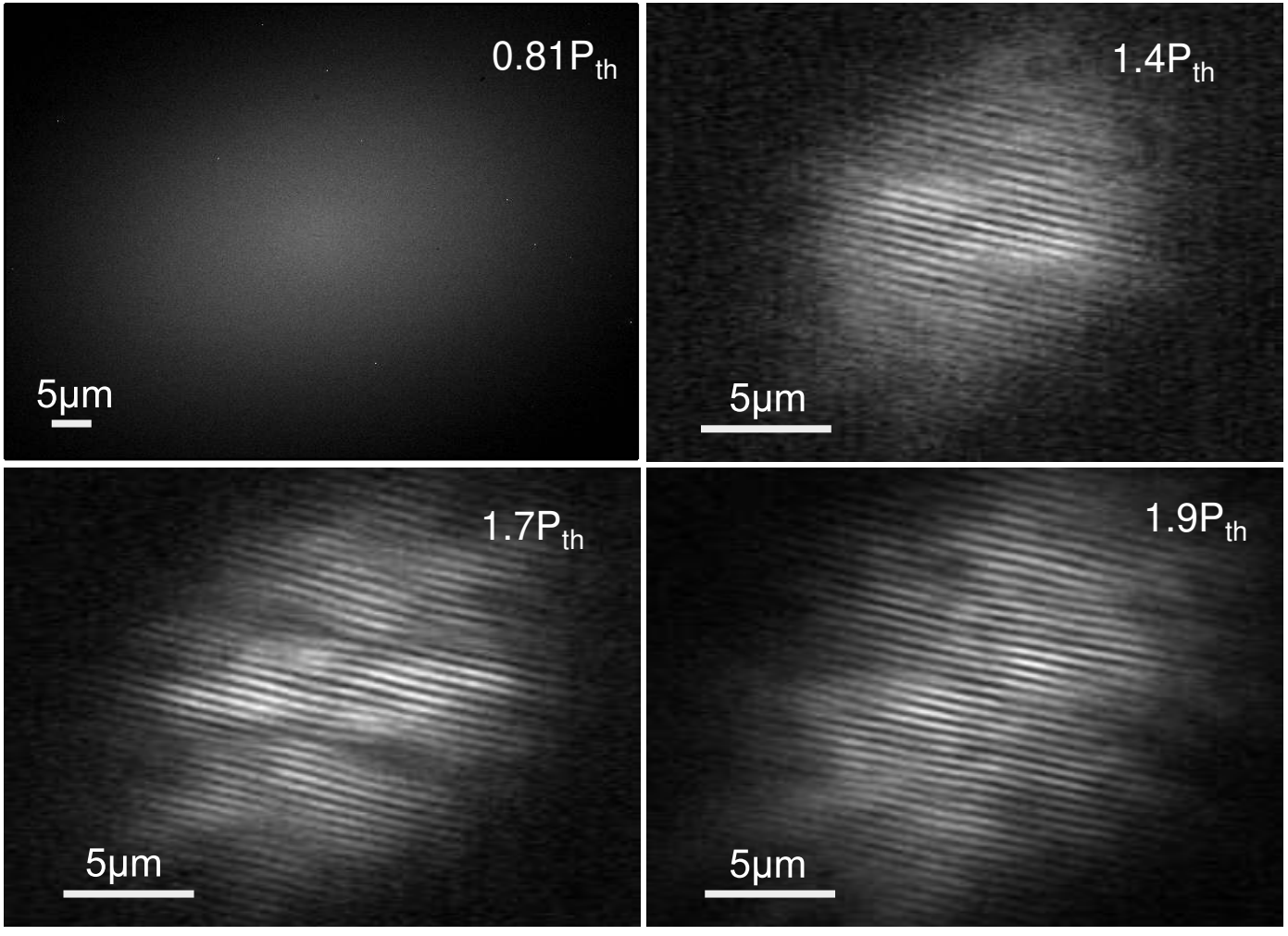

Figure 6